Imaging the surface stress and vibration modes of a microcantilever by laser beam deflection microscopy

Javier Tamayo[1], Valerio Pini[1], Prisicila Kosaka[1], Nicolas F. Martinez[2], O. Ahumada[2] and M. Calleja[1]

[1]Instituto de Microlectrónica de Madrid (IMM, CSIC), Isaac Newton 8 (PTM), Tres Cantos, 28760 Madrid, Spain
[2]MecWins, Santiago Grisolía 2 (PTM), Tres Cantos, 28760 Madrid, Spain

E-mail: jtamayo@imm.cnm.csic.es

Abstract

There is a need of non invasive techniques for simultaneous imaging of the stress and vibration mode shapes of nanomechanical systems in the fields of scanning probe microscopy, nanomechanical biological and chemical sensors, and semiconductor industry. Here we show a novel technique that combines a scanning laser, the beam deflection method and digital multifrequency excitation and analysis for simultaneous imaging of the static out-of-plane displacement and the shape of five vibration modes of nanomechanical systems. The out-of-plane resolution is of at least 100 pm/Hz$^{1/2}$ and the lateral resolution being determined by the spot size, is here of 1-1.5 µm. The capability of the technique is demonstrated by imaging the residual surface stress of a microcantilever together with the shape of the first 22 vibration modes. The vibration behavior is compared with rigorous finite element simulation. The technique is suitable to major improvements addressed to imaging in liquids, higher bandwidth measurements of nanoscale systems and enhanced spatial resolution.

S Online supplementary data available from stacks.iop.org/Nano/xxxxxxx
(Some figures may appear in colour only in the online journal)

1. Introduction

Cantilevers represent one of the most simple and ubiquitous mechanical structures used in engineering and by nature. Aircraft wings[1] and antennal mechanosensory organs of insects[2] are two prominent examples of the importance of the mechanical behaviour of cantilevers to perform their function. At the mid eighties of the last century, scientists realized that when the cantilevers are reproduced at the microscale, typically 0.2–1 μm thick, 20–100 μm wide, and 100–500 μm long, the cantilevers are able to deflect of the order of few nanometers in response to forces in the piconewton range, a range where concur the forces between atoms, molecules, and biomolecules that govern many of the physicochemical properties of materials as well as many fundamental life processes[3,4]. This concept is the heart of the atomic force microscope (AFM) invention: a sharp tip attached to the free end of a microcantilever scans a surface in a similar way to the stylus of a vinyl record player, for mapping the topography and intermolecular interactions coming from the surface. The corresponding microcantilevers deflections can be optically or electrically detected with a resolution of at least 100 pm/$Hz^{1/2}$. Batch fabrication of microcantilevers by adopting the well-established lithography and etching processes from semiconductor industry has enabled the fast and large expansion of the atomic force microscopy and created the optimum conditions for the development of biological and chemical nanomechanical sensors almost one decade later[5,6,7,8,9,10]. In these devices, tipless microcantilevers are coated on one side with a receptor layer that specifically binds the targeted molecules in gas or liquid phase. In this case, the in-plane forces that develop between the molecules at the cantilever surface give rise to a bending.

In addition to the static deformation of the cantilevers, the resonant frequencies have been also measured for gentle imaging of soft surfaces in AFM[11,12] and for developing cantilever sensors based on the added mass and stiffness of the molecules captured on the cantilever surface[13,14,15,16,17]. In both fields, there is an increasing interest in the use of higher resonant modes to enhance the sensitivity and the detection limits [18,19,20,21,22]. However, it is extremely complex to determine the vibration mode shape that corresponds to each resonant frequency[23], which is clearly important to quantify and interpret the measurements[14,21,22]. There are also long standing issues on the dynamic behavior of microcantilevers that have not been solved such as the effect of surface stress on the resonant properties[24,25] or the coupling between modes induced by the viscous damping, elastic elements or by intermittent contact[26,27,28]. The advent of finite element simulations and increasingly fast computer processing is shedding light to these questions. However, these simulations can be time-consuming and ignore the defects and imperfections inherent to the micro- and nanofabrication processes.

It is thus clear, that the development of non invasive optical tools for the characterization of the mechanical behaviour is becoming a need to obtain reliable results with nanomechanical systems and for the validation of micro- and nanofabrication processes.

Recently scanning Doppler laser vibrometry(SDLV) [29] and white light interferometry (WLI)[23,30,31] have demonstrated a significant ability for the characterization of nanomechanical systems. SDLV can image with high sensitivity the out-of-plane vibration of nanomechanical systems with sub-angstrom resolution and submicrometer lateral resolution. WLI provides information on the topography of nanomechanical systems with a vertical resolution of 1-10 nm. In addition, the implementation of stroboscopic illumination in WLI has enabled analysis of vibration modes, although the process is slow, the bandwidth is limited, and the resolution is still poor. In our opinion, there is a need for microscopy techniques that can simultaneous image the static and dynamic features of nanomechanical systems with high sensitivity and high resolution in a quick and simple manner.

Here, we present an optical microscopy technique based on the beam deflection method[32,33,34] that simultaneously provides a spatial map of the static deflection and shape of any five vibration modes of choice with sub-angstrom vertical resolution. We apply the technique to determine the spatial distribution of the surface stress and vibration shape of the first 22 eigenmodes of a gold-coated microcantilever sensor (Concentris). The cantilever is 500 µm long, 100 µm wide, and 1 µm thick.

2. The laser beam deflection microscopy technique

The experiments were performed by adapting the SCALA platform (MecWins) for multifrequency analysis[35,36]. The core of the laser beam deflection technique is the automated two-dimensional scanning of a laser beam across the surface of a nanomechanical system, in this case a microcantilever, and the collection of the reflected beam on the surface of a two-dimensional position sensing linear detector (PSD) orthogonally oriented to the reflected beam (Fig. 1(a)). We define a coordinate system in which the *X*-*Y* plane is the device plane and *X* and *Y* are along the scanning directions. Hence the out-of-plane displacement of the cantilever is along the *Z* axis. The incident laser beam is in the *X*– *Z* plane and the PSD is oriented with one axis along the *Y* direction. In this configuration, the photocurrents along the PSD axes (that are determined by the coordinates of the reflected laser beam on the PSD) are linearly proportional to the slope of the device surface along the *X* and *Y* directions at the point of reflection (Fig. 1(b)). The photocurrents are converted to voltage by current-to-voltage amplifiers in order to obtain three output voltages that give the *X* and *Y* slopes of the surface and the reflected intensity. Since the photocurrents are normalized with respect to the total photocurrent, the slope values are insensitive to intensity fluctuations and variations in the optical properties of the surface. In the experiments, we oriented the cantilever along the *X* direction, so the variations in the *X* and *Y* slope channels can be related to the flexural and torsional displacements of the cantilever.

For obtaining dynamic information, the cantilever was driven by a signal composed by the sum of five time-varying sinusoidal signals with different frequencies. In the experiments, the

frequencies were chosen to be at the frequency of five resonant vibration modes, and the amplitude of each frequency component was tuned to obtain similar amplitude responses in the cantilever (Fig. 2). The excitation voltage signal was applied across a piezoelectric bimorph placed near the cantilevers' bases. The method can be extended to more frequencies; however, we chose five frequencies in order to limit the amount of generated data. By implementing a digital lock-in detection, the raw data from the slope signals of the PSD are multiplexed in static, and in- quadrature amplitudes with respect to each frequency component of the driving force. Thus, in a single imaging scan, 23 images are obtained, which correspond to static *X* and *Y* slopes, reflectivity; and in-phase and quadrature amplitudes of the *X* and *Y* slopes at the five driving frequencies. After the scanning, the system defines a mask based on the reflected light intensity that provides the shape of the cantilever. This mask is applied to the static and dynamic components of the *X* and *Y* slopes in order to obtain the static and multifrequency surface normal vector. To reconstruct the topography and the shape of the five driven vibration modes, we adopt an iterative integration method used for image reconstruction in photometric stereo to calculate the height of the object from the normal vector data[36,37].

Figure 3 shows the resulting static topography and shape of five vibration modes obtained from a single scan consisting of 512 lines acquired at a rate of one line per second. The acquisition time per pixel is of about 2 ms. The topography data shows that the cantilever is bent down (from the gold to the silicon) about 22 µm. This bending is a consequence of the high residual compressive stress developed during the thermal evaporation of a 50 nm thick gold layer that in our case is used for functionalization with single stranded DNA for nucleic acid detection[38]. The five driving frequencies correspond with the 1^{st}, 6^{th}, 14^{th}, 17^{th} and 22^{th} eigenmodes of the cantilever. A remarkable feature of the technique is the large frequency span, from few kHz to around 1 MHz, exhibited by the dynamic characterization. This range can be still expanded by improving the bandwidth of the PSD readout electronics[39,40]. The frequencies were chosen in order to show the different ways in which a cantilever can vibrate. In addition to the well-known flexural vibration modes as those shown at 4.58 and 158.2 kHz corresponding with the1^{st} and 4^{th} flexural modes, and torsional vibration modes as that shown at 594.6 kHz corresponding with the 7^{th} torsional vibration mode, the cantilever can vibrate in more complex and unpredictable ways, like the U-shaped motion found at 825.1 kHZ or the drum-like vibration found at 1031 kHz. It is important to emphasize that although the use of higher vibration modes is advantageous in terms of sensitivity due to the higher both frequency and quality factor[18,20,22], the knowledge on the vibration mode shape is absolutely necessary for obtaining a quantitative measurement. For instance, in nanomechanical sensors, the quantification of the adsorbed mass and mechanical properties requires of the shape of the used vibration mode, which is usually approximated by applying the one dimensional Euler-Bernoulli equation[14,22]. However, this approach only keeps approximately valid for the first flexural and torsional cantilever eigenmodes[22].

2. Distribution of the residual surface stress

The surface stress is usually measured by applying the so-called ‘‘bending plate’’ method that consists in measuring the cantilever curvature and relating it to the surface stress by applying the Stoney’s equation[8,41]. This method assumes that for isotropic or cubic materials (as silicon and silicon nitride, most widely used materials in cantilever fabrication) the cantilever bends with uniform and isotropic curvature. The curvature is usually obtained by measuring the cantilever deflection at the free end and assuming parabolic deformation, or by measuring the cantilever deflection at few points along the longitudinal direction. An important limitation of this approach is that it neglects the effect of the clamping constriction, i.e., the method is only strictly applicable to plates that are unrestrained along their edges [41]. This constriction, as shown below, has profound implications in the quantification of the surface stress, and hence in the effectiveness of the ‘‘bending plate’’ method. Here we have derived the two-dimensional spatial distribution of the surface stress by calculating the local curvature and applying the Euler-Bernoulli relationship between bending moment and curvature. We split the surface stress into longitudinal and transversal components, σ_x and σ_y, which are related to the curvatures along and across the cantilever, κ_x and κ_y, through,

$$\left(\sigma_x, \sigma_y\right) = \frac{Eh^2}{1-\nu}\left(\kappa_x, \kappa_y\right) \qquad (1)$$

where E is the Young’s modulus of the cantilever, ν is Poisson’s ratio, and h is cantilever thickness. Figures 4(a) and (b) show the spatial map of the longitudinal and transversal components of the surface stress. The profiles of the longitudinal and transversal surface stress along the longitudinal cantilever axis are shown in fig. 4(c). The results clearly demonstrate that the surface stress is neither uniform across the cantilever nor isotropic. The absolute value of the longitudinal surface stress is maximal near the clamp and it decays up to reach a constant value at a distance from the clamp of about twice the cantilever’s width. Contrarily, we observe that the absolute value of transversal stress is zero at the clamp and it increases up to reach the asymptotic value of the longitudinal surface stress. This is in consistency with the model proposed by Sader, in which there exists a region near the clamp, with a length of the order of the cantilever´s width, where a non-uniform curvature exists[41]. In this region, nonzero in-plane stresses are developed that affect the resonance frequencies[24]. The fact that the transversal surface stress is zero at the clamp comes from the displacement restraint imposed by the clamp that induces a rigid body displacement in order to keep the transversal strain zero along the boundary between the cantilever and the chip base[24,41].

Finally, it is worth to note the noise of the curvature measurement due to the inherent noise produced by the numerical derivatives. In this context, the scanning laser beam deflection exhibits advantages for the quantification of the in-plane stresses in micromechanical

structures. When the out-of-plane displacement is directly measured, as it is the case of the interferometric techniques, the curvature calculation requires of the second derivative of the measurement that results into a two-step noise amplification. Advantageously, the beam deflection technique directly measures the slope, so it reduces the numerical derivation steps to one. Moreover, the laser-beam deflection is extremely sensitive, with noise below the 100 $pm/Hz^{1/2}$ that is about ten times smaller than the noise in white light interferometers, the standard technique for imaging static out-of-plane displacements in micromechanical structures.

3. Comparison between the experimental vibration mode shapes and finite element simulations

We have applied the implementation of the multifrequency excitation/detection technique in the scanning laser beam microscope for the characterization of the first 22 vibration modes of the microcantilever sensor. We split the vibration modes in flexural, torsional and U-shape. The experimental images of the first three modes of each category are shown at the top of figure 5. The resonance frequencies of the measured vibration modes are plotted at the bottom of figure 5. Based on our finite element simulations (FEM), one vibration mode was identified as the first lateral vibration mode (triangle symbol in fig. 5). Although this vibration mode consists on lateral motion of the cantilever in the XY plane, the simulations show that the lateral motion also induces a Z-displacement with a pattern very similar to that found experimentally (inset in the bottom of fig. 5). The details of the FEM simulations are provided in the supplementary material.

As shown in the previous section, the gold-coated side of the microcantilevers exhibits large surface stress that induces a significant cantilever bending. Previously, we reported that the surface stress induced resonant frequency shift has two components: i) a linear term related to the unreleased in-plane stresses near the clamp and ii) a non linear term related to the cantilever bending moment that is negative and approximately independent of the surface stress sign[25]. The contribution of each term depends on the vibration mode in a complex way. In order to compare the experiments with rigorous FEM, we introduced the effect of the surface stress in the FEM simulations. The simulations show that although the surface stress negligibly modifies the vibration mode shape in our conditions, it induces a significant frequency shift of the vibration modes as shown in figure 6 (top). Interestingly, the amount and sign of the frequency shift are related to the kind of motion. In general, the resonance frequencies of the flexural vibration modes slightly increase. This increase is of about 2% for the fundamental mode and it is getting smaller as flexural mode index increases. In contrast, the frequencies of the torsional vibration modes decrease by a significant amount, from 4 to 7% for the first five modes, following a complex dependence on the mode-index. The surface stress induced frequency shift of the U-shaped vibration modes is positive and it goes from 2% for the first mode to 4% for the second mode, and then it slightly decreases with the mode index. Interestingly, the lateral vibration mode exhibits the highest sensitivity to the surface stress, of

about 10%. Figure 6 (bottom) shows the deviation between the experimental and simulation values of the resonance frequencies. We find a good agreement (<5%) for the first six flexural and torsional modes. The deviation increases for the higher flexural modes, and it is significant for the U-shaped vibration modes, of about a 10%.

Finally, we show the images of the experimental vibration modes and the comparison with finite element simulations for the first ten vibration modes in figure 7. The rest of the measured vibration modes, up to the 22nd are shown in the supplementary data. Despite the differences in the values of the resonance frequency, the experimental images accurately follow the simulation data. The results show the ability of the presented technique to rapidly obtain the multimodal vibration shape of nanomechanical systems and the capability to link this dynamic behavior with the stress/strain field of the nanomechanical system.

4. Coclusions

In conclusion, we have developed a technique, so-called, scanning laser beam deflection microscopy for characterization of nanomechanical systems that enables the simultaneous imaging of the static out-of-plane displacement and several vibration modes in a simple and quick manner. The out-of-plane resolution is of at least 100 pm/Hz$^{1/2}$ and the lateral resolution that is determined by the spot size, is here of 1-1.5 µm. The multimodal characterization relies on synthesizing a driving waveform signal composed of several frequency components (at least five) together the digital lock-in multifrequency detection of the cantilever response. The capability of the technique is demonstrated by imaging the residual surface stress and shape of the first 22 vibration modes of a microcantilever sensor. The results reveal significant features of the mechanical response of microcantilever sensors that illustrate the capability of the presented technique. One relevant finding is that the surface stress cannot be quantified using the widely extended bending plate method as this method assumes uniform surface stress across the cantilever. The images show a region near the clamp, with a length of the order of the cantilever width's, where non-uniform curvature exists as it had been theoretically predicted. This effect seems to be the origin of the controversial issue about the influence of the surface stress on the resonance frequencies of singly clamped beams [24]. The rich and complex information obtained by the presented technique can be then compared to finite element simulations in order to gain further insight on the underlying mechanics of nanomechanical systems. Here, we found that whereas the experimental vibration mode shapes show little differences with the FEM simulations, the resonance frequencies significantly deviate from the FEM data for high vibration modes. In addition, the comparison between experimental data and FEM allows the identification of the first lateral vibration mode, that in principle it should not be perceptible as the in-plane motion negligibly influences on the laser beam deflection. However, the sensitivity of the technique allows the detection of the cross-talking between the in-plane and out-of-plane displacements. The technique is suitable to major improvements such as imaging in liquids addressed to biological applications as well as higher

acquisition bandwidth and enhanced spatial resolution addressed to extend the technique to nanoscale mechanical systems[29,42,43].

Acknowledgments.

The authors acknowledge financial support from the Spanish Science Ministry through projects ANEM! (TEC2009-14517-C02) and INMUNO-swing (IPT-2011-0821-010000); and from European Union through project NANOFORCELLS (ERC-StG-2011-278860). The authors acknowledge technical support from A. Salvador-Matar and R. Calleja (MecWins).

References

1. Scanlan RH, Rosenbaum R (1951) Aircraft vibration and flutter. The Kacmillan Company, New York.
2. Gnatzy W, Tautz J (1980) Ultrastructure and mechanical properties of an insect mechanoreceptor: stimulus-transmitting structures and sensory apparatus of the cereal filiform hairs of Gryllus. Cell and tissue research 213: 441-463.
3. Binnig G, Quate CF, Gerber C (1986) Atomic force microscope. Physical review letters 56: 930-933.
4. Gerber C, Lang HP (2006) How the doors to the nanoworld were opened. Nature nanotechnology 1: 3-5.
5. Fritz J, Baller M, Lang H, Rothuizen H, Vettiger P, et al. (2000) Translating biomolecular recognition into nanomechanics. Science 288: 316.
6. Gimzewski J, Gerber C, Meyer E, Schlittler R (1994) Observation of a chemical reaction using a micromechanical sensor. Chemical Physics Letters 217: 589-594.
7. McKendry R, Zhang J, Arntz Y, Strunz T, Hegner M, et al. (2002) Multiple label-free biodetection and quantitative DNA-binding assays on a nanomechanical cantilever array. Proceedings of the National Academy of Sciences 99: 9783.
8. Raiteri R, Grattarola M, Butt HJ, Skládal P (2001) Micromechanical cantilever-based biosensors. Sensors and Actuators B: Chemical 79: 115-126.
9. Thundat T, Warmack R, Chen G, Allison D (1994) Thermal and ambient-induced deflections of scanning force microscope cantilevers. Applied Physics Letters 64: 2894-2896.
10. Zhang J, Lang H, Huber F, Bietsch A, Grange W, et al. (2006) Rapid and label-free nanomechanical detection of biomarker transcripts in human RNA. Nature nanotechnology 1: 214-220.
11. García R, Perez R (2002) Dynamic atomic force microscopy methods. Surface science reports 47: 197-301.
12. Giessibl FJ (2003) Advances in atomic force microscopy. Reviews of modern physics 75: 949.
13. Verd J, Abadal G, Teva J, Gaudó MV, Uranga A, et al. (2005) Design, fabrication, and characterization of a submicroelectromechanical resonator with monolithically integrated CMOS readout circuit. Microelectromechanical Systems, Journal of 14: 508-519.
14. Tamayo J, Ramos D, Mertens J, Calleja M (2006) Effect of the adsorbate stiffness on the resonance response of microcantilever sensors. Applied Physics Letters 89: 224104.
15. Li M, Tang H, Roukes M (2007) Ultra-sensitive NEMS-based cantilevers for sensing, scanned probe and very high-frequency applications. Nature nanotechnology 2: 114-120.
16. Ilic B, Craighead H, Krylov S, Senaratne W, Ober C, et al. (2004) Attogram detection using nanoelectromechanical oscillators. Journal of Applied Physics 95: 3694.
17. Lavrik NV, Datskos PG (2003) Femtogram mass detection using photothermally actuated nanomechanical resonators. Applied Physics Letters 82: 2697.
18. Dohn S, Sandberg R, Svendsen W, Boisen A (2005) Enhanced functionality of cantilever based mass sensors using higher modes. Applied Physics Letters 86: 233501.
19. Proksch R (2006) Multifrequency, repulsive-mode amplitude-modulated atomic force microscopy. Applied Physics Letters 89: 113121.
20. Ghatkesar MK, Barwich V, Braun T, Ramseyer JP, Gerber C, et al. (2007) Higher modes of vibration increase mass sensitivity in nanomechanical microcantilevers. Nanotechnology 18: 445502.
21. Lozano JR, Garcia R (2008) Theory of multifrequency atomic force microscopy. Physical review letters 100: 76102.

22. Ramos D, Tamayo J, Mertens J, Calleja M, Villanueva L, et al. (2008) Detection of bacteria based on the thermomechanical noise of a nanomechanical resonator: origin of the response and detection limits. Nanotechnology 19: 035503.
23. Reed J, Wilkinson P, Schmit J, Klug W, Gimzewski J (2006) Observation of nanoscale dynamics in cantilever sensor arrays. Nanotechnology 17: 3873.
24. Lachut MJ, Sader JE (2007) Effect of surface stress on the stiffness of cantilever plates. Physical review letters 99: 206102.
25. Pini V, Tamayo J, Gil-Santos E, Ramos D, Kosaka P, et al. (2011) Shedding Light on Axial Stress Effect on Resonance Frequencies of Nanocantilevers. ACS nano.
26. Gil-Santos E, Ramos D, Jana A, Calleja M, Raman A, et al. (2009) Mass sensing based on deterministic and stochastic responses of elastically coupled nanocantilevers. Nano letters 9: 4122-4127.
27. Paul M, Clark M, Cross M (2006) The stochastic dynamics of micron and nanoscale elastic cantilevers in fluid: fluctuations from dissipation. Nanotechnology 17: 4502.
28. Rabe U, Janser K, Arnold W (1996) Vibrations of free and surface-coupled atomic force microscope cantilevers: Theory and experiment. Review of scientific instruments 67: 3281-3293.
29. Biedermann LB, Tung RC, Raman A, Reifenberger RG (2009) Flexural vibration spectra of carbon nanotubes measured using laser Doppler vibrometry. Nanotechnology 20: 035702.
30. Helm M, Servant J, Saurenbach F, Berger R (2005) Read-out of micromechanical cantilever sensors by phase shifting interferometry. Applied Physics Letters 87: 064101.
31. Kelling S, Paoloni F, Huang J, Ostanin VP, Elliott SR (2009) Simultaneous readout of multiple microcantilever arrays with phase-shifting interferometric microscopy. Review of scientific instruments 80: 093101.
32. Marti O, Colchero J, Mlynek J (1990) Combined scanning force and friction microscopy of mica. Nanotechnology 1: 141.
33. Meyer G, Amer NM (1990) Simultaneous measurement of lateral and normal forces with an optical-beam-deflection atomic force microscope. Applied Physics Letters 57: 2089-2091.
34. Mertens J, Álvarez M, Tamayo J (2005) Real-time profile of microcantilevers for sensing applications. Applied Physics Letters 87: 234102.
35. Martínez N, Kosaka P, Tamayo J, Ramírez J, Ahumada O, et al. (2010) High throughput optical readout of dense arrays of nanomechanical systems for sensing applications. Review of scientific instruments 81: 125109-125109-125109.
36. Kosaka P, Tamayo J, Gil-Santos E, Mertens J, Pini V, et al. (2011) Simultaneous imaging of the topography and dynamic properties of nanomechanical systems by optical beam deflection microscopy. Journal of Applied Physics 109: 064315.
37. Horn BKP (1990) Height and gradient from shading. International journal of computer vision 5: 37-75.
38. Mertens J, Rogero C, Calleja M, Ramos D, Martín-Gago JA, et al. (2008) Label-free detection of DNA hybridization based on hydration-induced tension in nucleic acid films. Nature nanotechnology 3: 301-307.
39. Enning R, Ziegler D, Nievergelt A, Friedlos R, Venkataramani K, et al. (2011) A high frequency sensor for optical beam deflection atomic force microscopy. Review of scientific instruments 82: 043705.
40. Rutten PE (2011) High speed two-dimensional optical beam position detector. Review of scientific instruments 82: 073705.
41. Sader JE (2001) Surface stress induced deflections of cantilever plates with applications to the atomic force microscope: Rectangular plates. Journal of Applied Physics 89: 2911.
42. Kiracofe D, Yazdanpanah M, Raman A (2011) Mass and stiffness calibration of nanowires using thermally driven vibration. Nanotechnology 22: 295504.

43. Gil-Santos E, Ramos D, Martínez J, Fernández-Regúlez M, García R, et al. (2010) Nanomechanical mass sensing and stiffness spectrometry based on two-dimensional vibrations of resonant nanowires. Nature Nanotechnology 5: 641-645.

FIGURES

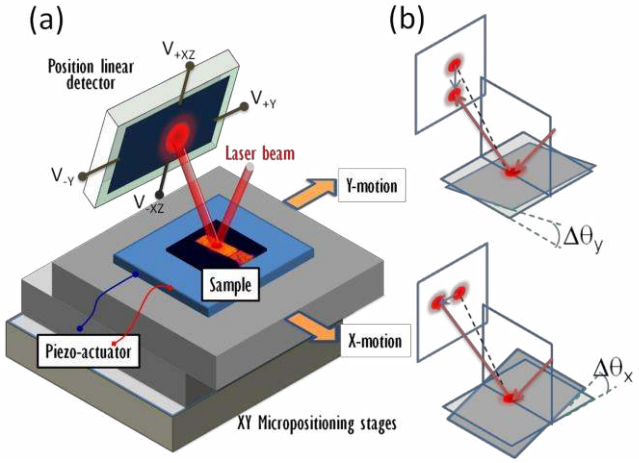

Figure 1. (a). Schematic representation of the scanning laser beam deflection system. A laser beam tightly focused on the surface of a nanomechanical system scans across its surface. The reflected beam is collected on the surface of a two-dimensional position linear photodetector (PSD). (b) Schematic representations of the displacement of the reflected laser beam on the PSD due to a change of the sample slope around the Y-axis and X-axis.

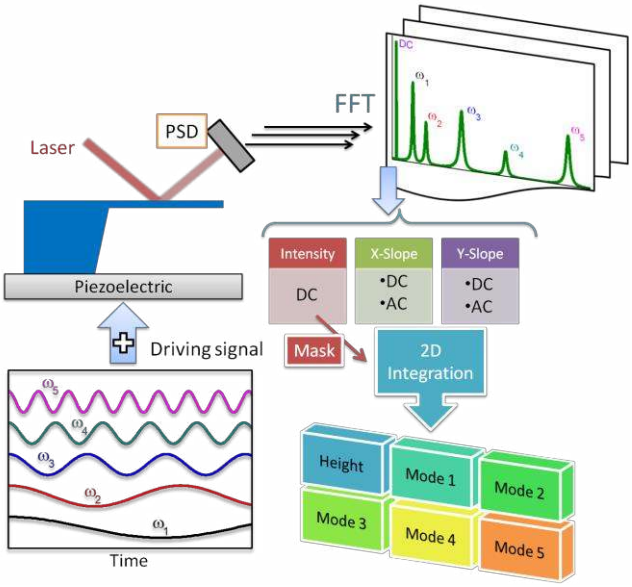

Figure 2. Schematic representation of the multifrequency excitation/detection in the scanning laser beam deflection microscope. A driving waveform signal consisting in the sum of five sinusoidal signals at different frequencies is synthesized. The frequencies are chosen to be at the resonant frequency of different vibration modes. A fast Fourier transform of the PSD channels corresponding with the X-slope and Y-slope of the sample reveal the static and multimodal out-of-plane displacements. The intensity PSD channel is used as a mask to obtain the cantilever shape. To reconstruct the topography and the shape of the five driven vibration modes, we adopt an iterative integration method.

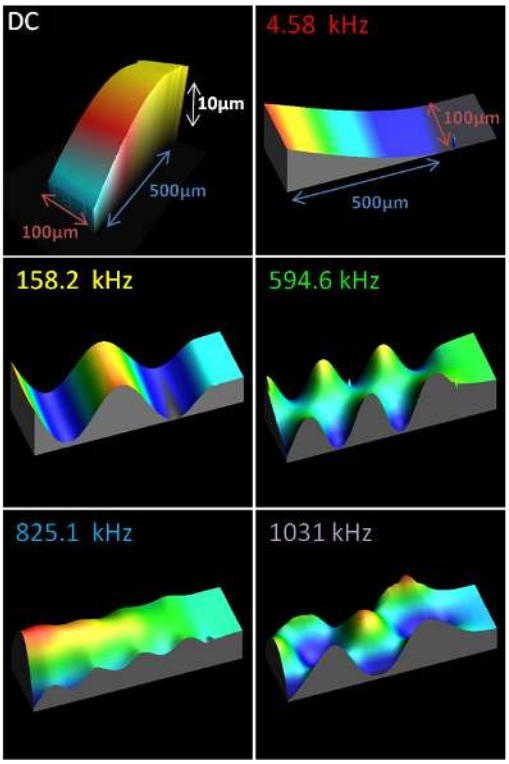

Figure 3. Simultaneous detection of the static out-of-plane displacement and the shape of five vibration modes of a microcantilever sensor.

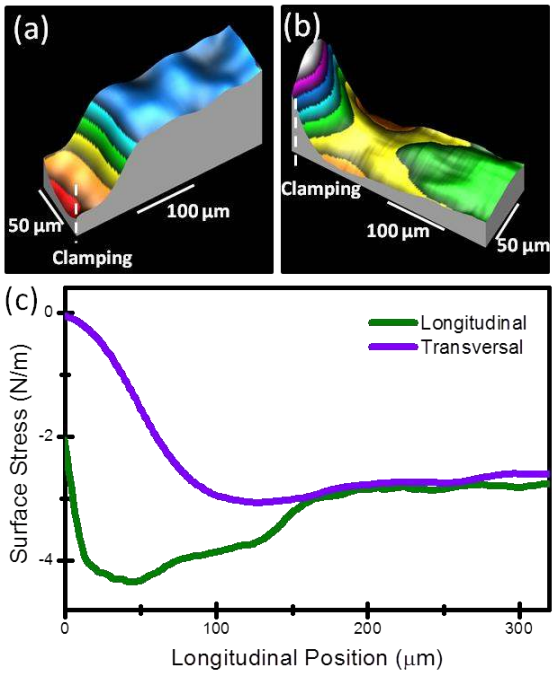

Figure 4. Images of the longitudinal (a) and transversal (b) components of the differential surface stress derived from the corresponding curvatures. The images are 320 µm long and 70 µm wide. This size is chosen in order to highlight the cantilever region near the clamping where there are non-uniform curvatures and to exclude the cantilever edges where the curvature measurement is very nosy.

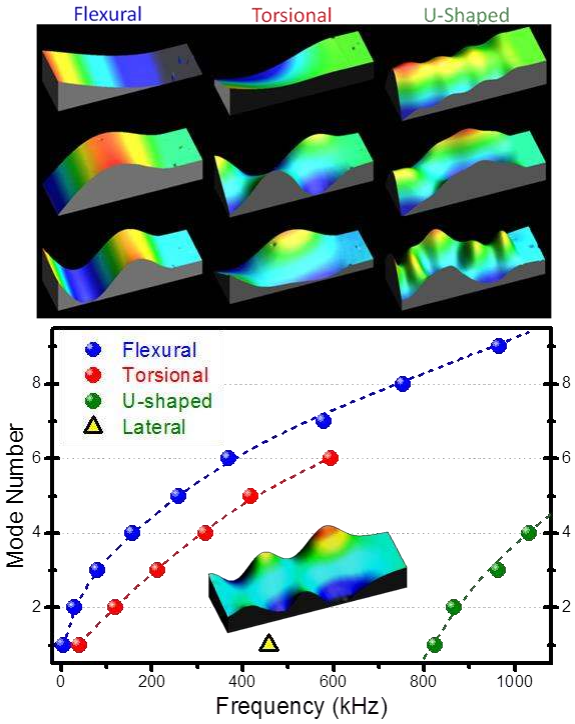

Figure 5. Top. Images of the first three vibration modes in which the vibrations consist of flexural, torsional and U-shaped motion. Bottom. Experimental values of the resonance frequencies of the first 20 vibration modes of a microcantilever sensor. The frequencies are split into flexural, torsional, U-shaped and lateral vibration modes. The inset in the graph shows the out-of-plane displacement of the first lateral vibration mode as a consequence of the cross-talking between in-plane and out-of-plane displacements.

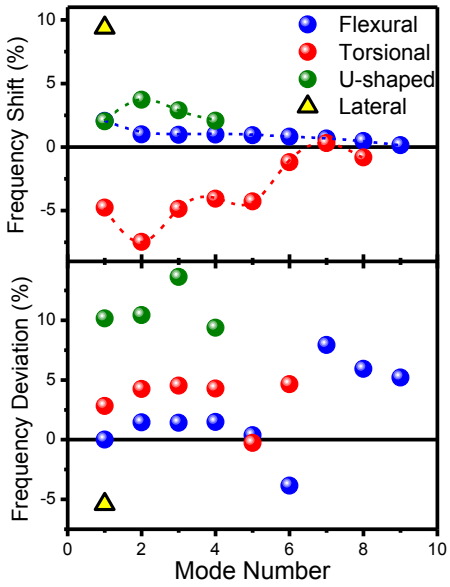

Figure 6. The graph at the top shows the FEM simulations of the surface-stress induced shift in the resonance frequencies of the microcantilever sensor examined here. In order to simulate the surface stress, cantilever was subject to a change in the temperature in order to obtain a bending similar to that found experimentally. The graph at the bottom shows the deviation between the experimental values of the resonance frequencies and the FEM data. The vibration modes are arranged in flexural, torsional, U-shaped and lateral modes (see text and fig. 5).

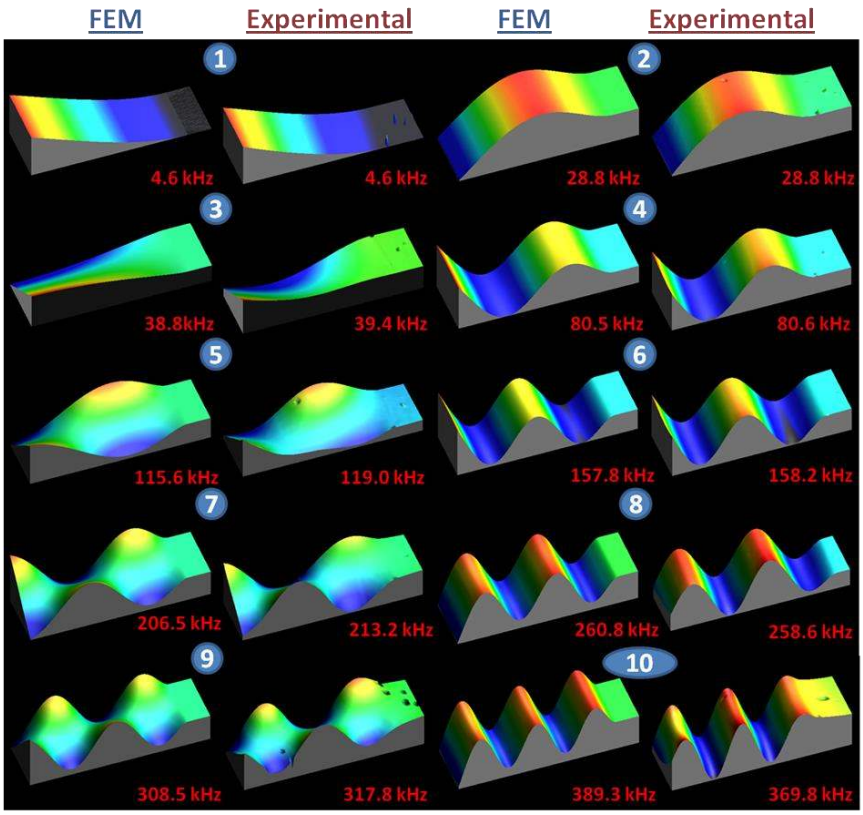

Figure 7. Comparison between the experimental shape of the first ten vibration modes and the FEM simulations.

SUPPORTING INFORMATION

Imaging the surface stress and vibration modes of a microcantilever by laser beam deflection microscopy

Javier Tamayo[1], Valerio Pini[1], Prisicila Kosaka[1], Nicolas F. Martinez[2], O. Ahumada[2] and M. Calleja[1]

[1]*Instituto de Microlectrónica de Madrid (IMM, CSIC), Isaac Newton 8 (PTM), Tres Cantos, 28760 Madrid, Spain*

[2]*MecWins, Santiago Grisolía 2 (PTM), Tres Cantos, 28760 Madrid, Spain*

E-mail: jtamayo@imm.cnm.csic.es

FEM SIMULATION

The natural frequencies and mode shapes of the microcantilever sensors were simulated by the finite element method (FEM) using the commercial software Comsol 4.2. A gold-coated cantilever of length 500 µm, width 100 µm, and substrate and coating thicknesses of 950 nm and 50 nm, respectively was modeled. These dimensions are the nominal dimensions of the microcantilever sensor used in the experiments. Since the microcantilever is fabricated in monocrystalline silicon with the edges along the <110> direction, we used in the simulations an anisotropic elasticity model that accurately describes the silicon elasticity [1]. The simulation process consisted of two sequential steps. First, we calculated the static cantilever strains when the cantilever is subject to a uniformly distributed temperature change. The temperature value is chosen in order to achieve a cantilever bending due to the bimetallic effect similar to that experimentally found due the residual stress generated in gold coating. The simulations include large deformation effects that arise from the geometric nonlinearity. Thus, the Green strain tensor and the second Piola Kirchhoff stress tensors are used and the solution is achieved by using a total Lagrangian formulation. In the second simulation step, we obtain the cantilever eigenfrequencies by including the static cantilever deformation previously obtained in the first simulation step. In order to avoid time-consuming inefficient calculations and to achieve accurate solutions, the meshing of the cantilever structure is individually adapted to each

direction. We applied a customized free tetrahedral meshing. In addition, since the stress and strain near the clamping region play a critical role in the vibration response of the cantilevers, the meshing of this regionn was refined with an extremely fine meshing. A convergence study was performed by refining the mesh element size until the relative error in the cantilever eigenfrequency was below 10^{-4}. This corresponds to a mesh of 500 000 elements, approximately.

[1] Matthew A. Hopcroft, Member, IEEE, William D. Nix, and Thomas W. Kenny, What is the Young's Modulus of Silicon? JOURNAL OF MICROELECTROMECHANICAL SYSTEMS, VOL. 19, NO. 2, APRIL 2010

COMPARISON BETWEEN THE EXPERIMENTAL AND SIMULATED VIBRATION MODES

The manuscript shows the images of the experimental vibration modes and the comparison with finite element simulations for the first ten vibration modes (figure 7). The rest of the measured vibration modes, up to the 22^{nd} are shown here (Fig. S1). Despite the differences in the values of the resonance frequency, the experimental images accurately follow the FEM data. Only two vibration modes (based on the FEM simulations) were not detected, 16^{th} and 17^{th}. We relate this to the frequency overlapping of the resonance peaks of these modes with neighboring vibration modes that are more efficiently excited by the piezoelectric actuator.

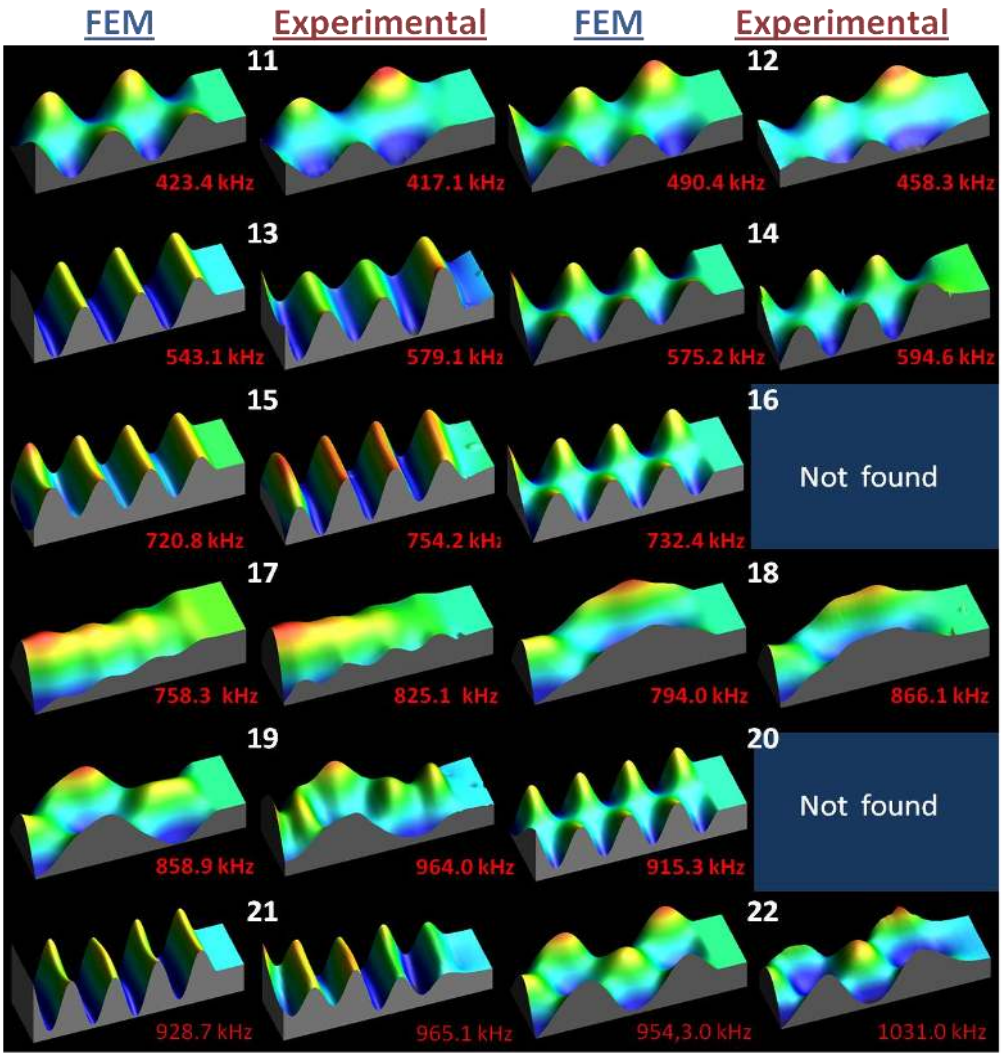

Figure S1. Comparison between the experimental shape of the vibration modes from the 11th to the 22nd and the FEM simulations.